# Modeling and Analyzing Copper Dendrite Growth during Electrochemical Migration Using Monte Carlo Simulation

Ali Gharaibeh, Ali Dayoub, Balázs Illés, and Bálint Medgyes
Department of Electronics Technology, Faculty of Electrical Engineering and Informatics, Budapest University of Technology and Economics, Műegyetem rkp. 3., H- 1111 Budapest, Hungary
ali.gharaibeh@vik.bme.hu

*Abstract*—Electrochemical migration (ECM) has recently received increased attention, primarily due to the escalating risk of short circuits associated with the continuous miniaturization of microelectronic devices. As the spacing between conductive elements decreases, the likelihood of ECM-induced failures rises, necessitating a deeper understanding of the underlying mechanisms. This study presents a 2D computational model designed to simulate the ECM process in Cu. The model deterministically accounts for the anodic dissolution of Cu and the subsequent ion transport, while the stochastic nature of dendritic growth is captured through Monte Carlo simulation. To validate the accuracy and reliability of the proposed model, a series of water-drop (WD) tests were conducted using pure copper electrodes separated by a 200 µm gap distance, subjected to a constant 10 VDC bias, and a droplet from a contaminant-free electrolyte. The findings emphasize the versatility of Monte Carlo simulation in accurately replicating ECM behavior in Cu-based systems. By fine-tuning key simulation parameters, the model successfully predicts the Time-to-Failure (TTF) and effectively captures the characteristic tree-like morphology of Cu dendrites.

*Keywords—electrochemical migration, microelectronics reliability, numerical modeling, Monte Carlo simulation*

## I. INTRODUCTION

Electrochemical migration (ECM) is a prevalent reliability concern in modern microelectronics. This phenomenon, driven by humidity, arises from specific electrochemical corrosion processes. Ultimately, it leads to short-circuit failures between adjacent electrodes with opposite biases [1]. ECM occurs through four sequential stages: (i) the formation of an electrolyte layer on the substrate through the absorption or condensation of water molecules; (ii) the dissolution of metal atoms from conductor layers or solder joints at the anode, where these atoms oxidize, releasing electrons and forming cations; (iii) the movement of ions via diffusion, migration, and convection; and (iv) the reduction of metal ions at the cathode, resulting in dendrite growth through reduction processes [2]. The most used parameter to assess this risk is the Time-to-Failure (TTF), which indicates the system's susceptibility to ECM [3]. TTF is significantly influenced by factors such as the type of metal, the applied bias voltage, the spacing between metal surfaces, and the presence of contaminant ions in the water. ECM is receiving growing attention in the microelectronics industry as ongoing miniaturization trends heighten the likelihood of this failure mechanism occurring.

The ECM phenomenon has been extensively studied through experimental research [1]–[3]. However, numerical modeling of ECM is essential for predicting failure risks, optimizing designs, and improving the reliability of microelectronics. This approach allows for the simulation of complex interactions involving factors such as humidity, voltage, and material properties. Despite this, the literature contains only a limited number of numerical simulation studies focused on exploring ECM [4]. This may be attributed to the fact that most developed models focus on simulating electrochemical deposition processes in electrochemistry rather than specifically addressing ECM. He et al. [5] illustrate the differences between electrochemical deposition processes and ECM by comparing them to their developed 1D model for ECM of Cu, demonstrating that existing models have limited accuracy in modeling ECM. They successfully modeled the ion transport step by numerically solving the Nernst-Planck equation using the finite difference method (FDM), obtaining an exponential ion concentration profile along the gap distance. However, their model did not account for dendrite growth.

In contrast, Illés et al. [6] developed a 2D model to simulate the growth of Cu dendrites by introducing a self-developed algorithm based on ion concentration along the gap distance, successfully capturing both dendrite growth and the entire ECM process. Additionally, Ma et al. [7] used the finite element method (FEM) to numerically solve the Nernst-Planck equation, explaining the dominance of Sn in dendrites formed at 3V and Zn in dendrites formed at 5V during ECM of Sn-9Zn in deionized (DI) water. Furthermore, Ható et al. [8] introduced Brownian Dynamics (BD) simulations to model the electrodiffusion of Sn ions and dendrite growth at a molecular level. Their simulations revealed that higher ion concentrations and stronger electric fields accelerate dendrite growth, providing insight into why dendrite growth speeds up as dendrites approach the anode. Moreover, Cao et al. [9] employed a phase-field model to reproduce the morphology of silver dendrites and identify the critical voltage phenomenon observed in water drop (WD) experiments. Additionally, Dayoub et al. [10] introduced a unique approach by using Monte Carlo simulations to model the growth of Cu dendrites, incorporating ion concentration and electric field values on a 2D grid. Building on previous research, this work aims to provide deeper insights into modeling TTF and the growth of Cu dendrites by leveraging the flexibility of Monte Carlo simulations.

## II. NUMERICAL SIMULATION OF ECM PROCESSES

The steps of the ECM process of Cu are illustrated schematically in Fig. 1.

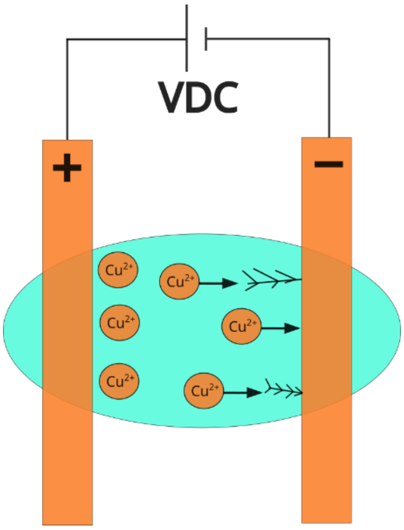

Fig. 1. Schematic illustration of the ECM process for Cu (anode is on the left and cathode is on the right).

### A. *Anodic Dissolution*

The ECM process initiates with the dissolution of copper at the anode, leading to the direct formation of $Cu^{2+}$ ions at the anode [11], as represented by (1). When the applied bias voltage is high enough, oxygen evolution resulting from water dissociation also occurs at the anode surface [1], as described in (2).

$$Cu \rightarrow Cu^{2+} + 2e^{-} \tag{1}$$

$$2H_2O \rightarrow O_2 + 4H^{+} + 4e^{-} \tag{2}$$

The anodic dissolution produces an amount of Cu ($c_{an}$) that can be approximated using a combination of Faraday's law and Ohm's law [10], as described in (3).

$$c_{an} = \frac{\varphi_{an} \times (\sigma_0 + c \times q \times \mu) \times M}{n \times F \times V_{droplet}} \times \Delta t \tag{3}$$

Here, $\varphi_{an}$ represents the applied DC potential at the anode (10V), $\sigma_0$ signifies the electrical conductivity of DI water ($0.055\times10^{-6}$ S/m), c stands for the concentration of $Cu^{2+}$ ions, and q represents the charge of $Cu^{2+}$ ions, given by n×e, where n is the chemical valence of $Cu^{2+}$ ions (+2), and e is the elementary charge ($1.6\times10^{-19}$ C). Additionally, μ refers to the mobility of $Cu^{2+}$ ions ($5.56\times10^{-8}$ $m^2/Vs$), M indicates the molar mass of $Cu^{2+}$ ion (63.54 g/mol), Δt indicates the simulation time step (350 μs), F is the Faraday constant (96 485.3321 C/mol), and $V_{droplet}$ corresponds to the volume of the DI droplet (15 μl).

### B. *Ion Transport*

Within the interior region (i.e., gap distance) where ion transport takes place, the potential distribution is governed by Poisson's equation for electrostatics. However, due to the electroneutrality condition in the droplet, the net charge density (ρ) is effectively zero [7]. This simplifies Poisson's equation to Laplace's equation. Thus, the potential distribution and the electric field in the gap distance can be determined using (4) and (5), respectively. Additionally, in the context of ion transport, the impact of electroconvection on overall transport in ECM is negligible [12]. Consequently, $Cu^{2+}$ ions generated at the anode mainly transport through the electrolyte toward the cathode under the effect of diffusion and migration, as described by the Nernst–Planck equation (6). In the absence of homogeneous reactions, the transient changes in $Cu^{2+}$ ion concentration within the electrolyte droplet are governed by the continuity equation, (7), allowing for the calculation of $Cu^{2+}$ ion concentrations across the computational grid as in (8).

$$\nabla^2\varphi = \frac{\partial^2\varphi}{\partial x^2} + \frac{\partial^2\varphi}{\partial y^2} = 0 \tag{4}$$

$$\bar{E} = -\nabla\varphi \tag{5}$$

$$\bar{J} = -D\nabla c - \mu c\nabla\varphi \tag{6}$$

$$\frac{\partial c}{\partial t} = -\nabla . J \tag{7}$$

$$\frac{\partial c}{\partial t} = D\nabla^2 c + \mu\nabla c . \nabla\varphi \tag{8}$$

Here, J represents the mass flux of $Cu^{2+}$ ions, while D denotes the diffusion coefficient of $Cu^{2+}$ ions ($3.67\times10^{-10}$ $m^2/s$).

### C. *Dendrite Growth*

Dendrite growth begins with the electrochemical reduction of transported $Cu^{2+}$ ions at the cathode [13], as described in (9), followed by successive reductions occurring both at the cathode and on the already-formed dendrites. Consequently, dendrites act as dynamic cathodes, requiring adjustments to the electric potential and electric field ((4) and (5)) after each reduction step. In addition to (9), the reduction of water also takes place [1], as described in (10).

$$Cu^{2+} + 2e^- \rightarrow Cu \tag{9}$$

$$2H_2O + 2e^- \rightarrow H_2 + 2OH^- \tag{10}$$

The reduction of water and oxygen evolution (2, 10) enhances droplet conductivity and creates a pH gradient for ion transport [14]. However, the ECM model considers only Cu dissolution (1) for anodic dissolution and Cu reduction (9) for dendrite growth. On one hand, the impact of (2, 10) on the overall conductivity of the droplet has been reported to be less significant compared to (1) [6]. Additionally, excluding them would significantly reduce the computational cost of the code.

The numerical model for dendrite growth combines random walk and Monte Carlo simulation to capture the stochastic nature of the process. Growth begins at the cathode, where metal atoms deposit once a critical ion concentration accumulates, forming tiny nuclei. These nuclei grow unevenly due to local fluctuations in ion concentration, electric field variations, and randomness. After initiation, a random starting point near the cathode is selected, and the object-oriented method move(x, y) displaces the point in the x or y direction until it encounters an existing dendrite. The method is_contact(dendrites, x, y) checks whether the new site is adjacent to an existing dendrite, ensuring that growth follows a branching pattern. Once contact is confirmed, the probability of dendrite growth at that location is determined using the method growth_probability(concentration), which calculates growth likelihood based on the local ion concentration as outlined in (11). During each dendrite growth attempt (N), a random number between 0 and 1 is generated to determine whether growth occurs. If this number is less than the growth probability calculated by the growth_probability function, a new dendrite site forms, allowing the structure to propagate. This approach effectively captures the stochastic and irregular nature of dendrite evolution observed in electrochemical systems.

$$growth\_probability\ (c)\ =\ \mathrm{k}\times\frac{c}{c_{max}} \qquad (11)$$

Here, k is the constant of the normalized $Cu^{2+}$ ion concentration across the grid, while $c_{max}$ represents the maximum $Cu^{2+}$ ion concentration ($7.56 \times 10^{-5}$ g/l) achievable at the anode due to dissolution in DI water at 293 K. This theoretical value, proposed in [6], has been successfully implemented in previous studies [6], [10] to normalize the concentration across the grid. However, unlike the model proposed in [6], the current 2D ECM model does not include a thickness parameter in the third direction (z-axis). Instead, the Monte Carlo method performs multiple N at randomly selected sites during each simulation step. If dendrite growth occurs at a specific site, the local concentration of $Cu^{2+}$ ions is set to zero, as the ions are consumed in the formation process. Similarly, the electric field at that point is also set to zero to reflect the metallic nature of the dendrites. The simulation proceeds iteratively until a dendrite reaches the anode, indicating a system failure.

### D. *Grid Specification and Parameters*

The 2D computational grid was created by meshing a fixed number of points in both the x and y directions, with nx = 200 points and ny = 200 points, respectively. The spacing between each point in the x-direction ($\Delta x$) is equal to the spacing in the y-direction ($\Delta y$), with both set to $\Delta x = \Delta y = h = 1\ \mu m$. The partial differential equations (4, 5, and 8) were numerically converted and discretized using the FDM. The computational ECM model was then built and executed in the Python programming language.

The selection of $\Delta t$ is governed by the Courant–Friedrichs–Lewy (CFL) condition [15]. For diffusion and migration, the system remains stable when constraints (C1) and (C2) are satisfied:

$$\Delta t_{diff} \leq \frac{h^2}{4D} \qquad (C1)$$

$$\Delta t_{mig}\ \leq\ \frac{h}{\mu E_{max}} \qquad (C2)$$

Here, $E_{max}$ represents the maximum electric field, given by ($\varphi_{an}$/d) where d is the gap distance (200 μm). Consequently, $E_{max}$ is $50\times10^{3}$ V/m Therefore, setting $\Delta t = 350$ μs ensures the numerical stability of the system.

### E. *Initial and Boundary Conditions*

Table 1 presents the initial and boundary conditions, while Fig. 2 depicts the simulation workflow for ECM of Cu.

TABLE I. APPLIED CONDITONS USED IN THE MODEL

| **Applied Conditions** | **Electrodes** | **φ [VDC]** | **Concentration of $Cu^{2+}$ ions [g/l]** |
|---|---|---|---|
| Initial | Anode | 10 | 0 |
| | Cathode | 0 | 0 |
| Boundary | Anode | 10 | $C_{an}^{n-1} + C^{*}_{an}$ |
| | Cathode | 0 | $C_{cath-1}^{n-1}$ |

*n denotes the simulation step, whereas $C_{an}$ is computed at each n based on (3)

```
Initialize simulation parameters, grid, and variables
SET initial conditions for electric potential (phi), ion concentration (c)
DEFINE move(x, y): RANDOMLY adjust (x, y) within bounds
DEFINE is_contact(dendrites, x, y): RETURN True if adjacent to dendrite
DEFINE growth_probability(c): RETURN c/cmax
FOR each time step:
    STORE previous values (c_prev, phi_prev)
    FOR each interior grid point: COMPUTE phi, Ex, Ey
    COMPUTE anodic dissolution ($c_{an}$)
    UPDATE anodic concentration s.t $c_{an} \leq$ cmax
    FOR each interior grid point: COMPUTE and UPDATE c
    APPLY cathode boundary condition
    IF time >= start_time AND not initiated: INITIATE dendrites
    # Monte Carlo dendrite growth
    IF dendrites growing:
        FOR growth attempts:
            SELECT random (x, y), MOVE until contact
            IF random() < growth_probability(c[x, y]): GROW dendrite
        IF dendrites reach anode: PRINT failure, SAVE plot, EXIT
    IF time step % 100 == 0: SAVE and DISPLAY dendrite structure
END simulation
```

Fig. 2. Simulation workflow for modeling ECM of Cu.

## III. RESULTS AND DISCUSSION

### A. *Validation of TTF*

Fig. 3 represents experimental TTF data derived from WD tests and computed TTF data generated using a wide range of N and k combinations. The experimental data exhibit noticeable variability, while the computed TTF values demonstrate different levels of variability depending on the values of N and k. When N is small (e.g., 5 or 10), the computed TTF values show high variability, indicating that smaller dendrite growth attempts contribute to greater uncertainty in the results. In contrast, as N increases (e.g., 50 or 70), the variability in computed TTF values decreases significantly, indicating that the computation of TTF values approaches deterministic behavior. This trend is further observed when N is randomized within a broader range, such as from 1 to 50, where the influence of randomness is restricted by including larger values. However, when N is randomized within a narrower range (e.g., 1 to 15), the TTF values still exhibit notable variability, indicating that a limited range of N can contribute to variability in the computed results. Furthermore, randomizing the value of k did not result in significantly larger variability, suggesting that the impact of k on TTF variability is less pronounced compared to N. These findings highlight the impact of dendrite growth attempts on the variability of TTF predictions.

Therefore, it can be concluded that the variability of the computed TTF is mainly governed by randomizing N, which may also reflect the experimental deviations. However, the greater variability observed in experimental TTF values may arise from several factors. One significant source of uncertainty is the contact area between the electrode and the electrolyte drop [3], which cannot be precisely controlled in each WD test. Variations in contact area directly influence the current density, leading to differences in TTF values. Additionally, hydrogen gas evolution at the cathode has been reported to contribute to the suppression of dendrite growth through both physical and chemical mechanisms [16]. Physically, hydrogen bubbles disrupt ion transport, creating uneven dendrite structures. Chemically, the generation of hydroxide ions increases the local pH, further influencing dendrite formation.

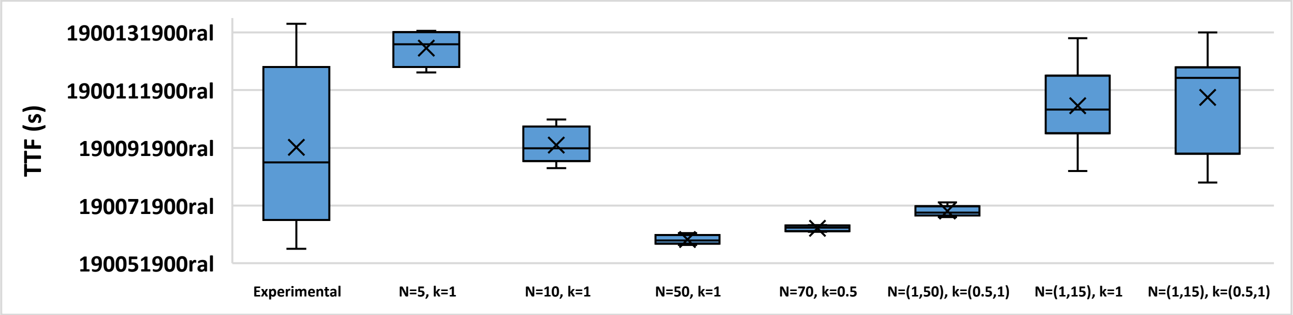

Fig. 3. Comparison of TTF data from experimental and computed WD tests (x represents the mean time to failure).

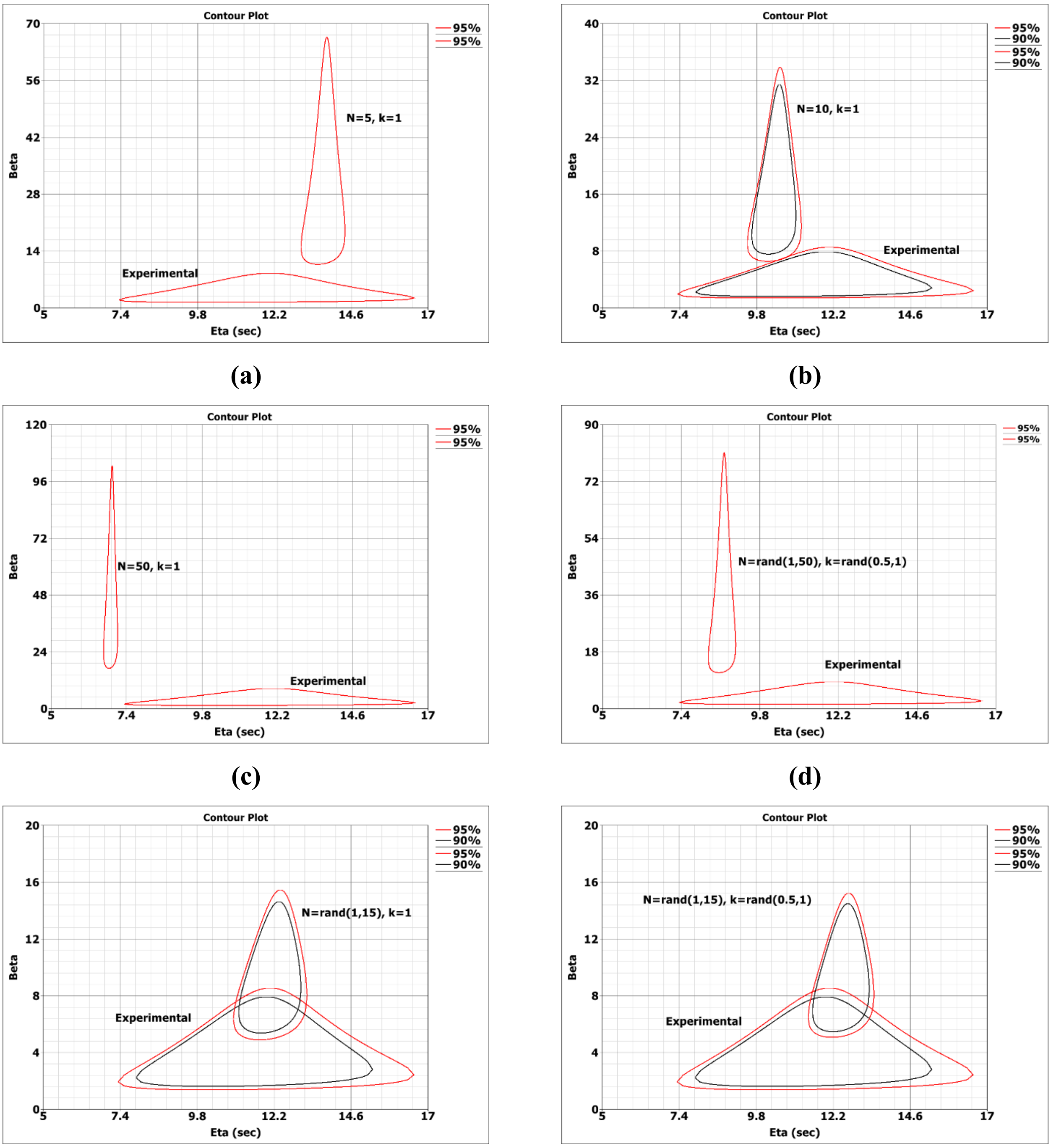

**(a)** **(b)**

**(c)** **(d)**

**(e)** **(f)**

Fig. 4. Contour plots comparing experimental TTF with computed TTF at 95% and 90% confidence levels to assess statistical significance for (a) N=5, k=1, (b) N=10, k=1, (c) N=50, k=1, (d) N=rand(1, 50), k=rand(0.5, 1), (e) N=rand(1, 15), k=1, and (f) N=rand(1, 15), k=rand(0.5, 1), where beta represents the shape parameter and eta represents the scale parameter in the Weibull distribution.

The efficiency of the computational model's TTF predictions is evaluated using contour plots in Fig. 4, where the overlap between experimental and computed TTF datasets determines statistical significance [17], [18]. The absence of overlap at a given confidence level indicates a significant difference. Fig. 4a shows no overlap at 95% confidence, meaning N=5, k=1 has a significantly higher TTF than experimental data. Similarly, Fig. 4b shows overlap at 95% but not at 90%, suggesting N=10, k=1 differs significantly at 90%. For larger N values (N=50, k=1 and randomized N=rand(1, 50), k=rand(0.5, 1)), Figs. 4c and 4d show no overlap at 95%, confirming significant differences. However, for smaller randomized ranges (N=rand(1, 15), k=1 and N=rand(1, 15), k=(0.5, 1), shown in Figs. 4e and 4f), contours overlap at both 95% and 90%, indicating no significant difference. These results suggest that the ECM of Cu is better modeled with a randomized N rather than a deterministic value.

### B. *Validation of dendrite morphology*

Fig. 5 presents a comparison between the experimental and computed dendrite morphologies for Cu. The experimental (Figs. 5a and 5b) and computed dendrites (Figs. 5c and 5d) showed good agreement, regardless of whether N and k were deterministic or randomized.

In both cases, the dendrites exhibit a fractal-like, tree-like morphology, initiating primarily from a single branch at the cathode and growing toward the anode. As they approach the anode, the dendrites become denser and display a more pronounced fractal-like structure, further highlighting the similarity between the experimental and computed results. This similarity in dendrite morphology can be further explained by the presence of one or two main dendritic branches, which primarily result from the primary branches consuming the majority of the surrounding $Cu^{2+}$ ions.

### C. *Exponential Growth of Dendrites*

Fig. 6 illustrates the growth of Cu dendrites at selected time intervals, providing insight into their evolution over time. The fitting of the main branch length, shown in Fig. 6d, demonstrates a strong exponential trend, suggesting that dendrite growth follows an exponential pattern. This observation aligns with previous findings reported by [6], despite differences in the underlying growth mechanisms. The exponential nature of dendrite growth may be attributed to the ionic concentration profile along the gap distance from the anode to the cathode, which has been shown to decrease exponentially, as reported in [5], [6], [10]. Consequently, the dendrite growth rate follows a similar exponential pattern.

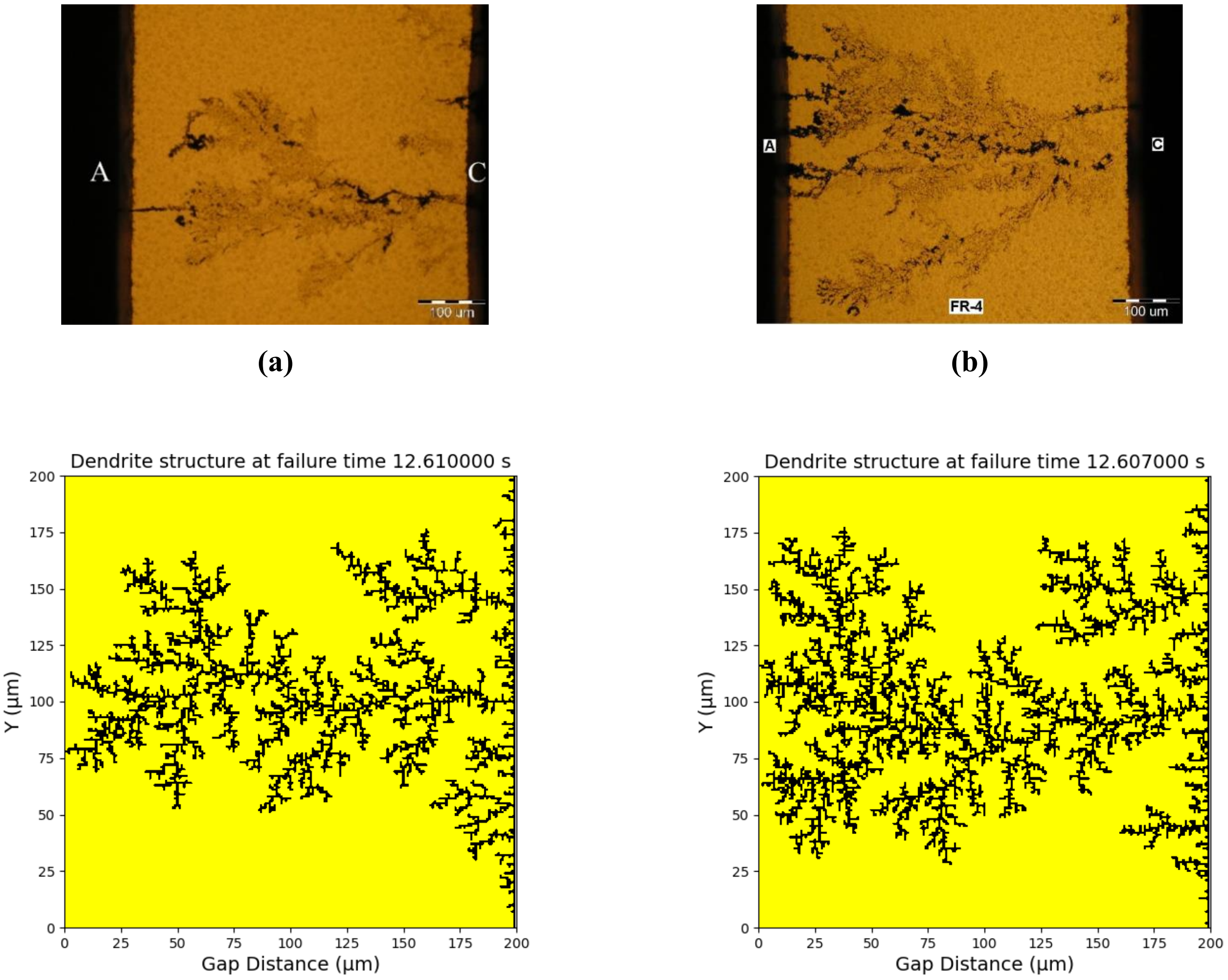

**(a)** **(b)**

**(c)** **(d)**

Fig. 5. Experimental and computed Cu dendrites at 10VDC in a DI water droplet. (a, b) Experimental dendrites, where A represents the anode and C represents the cathode and (c, d) Computed dendrites, where 0 μm gap distance represents the anode and 200 μm represents the cathode .

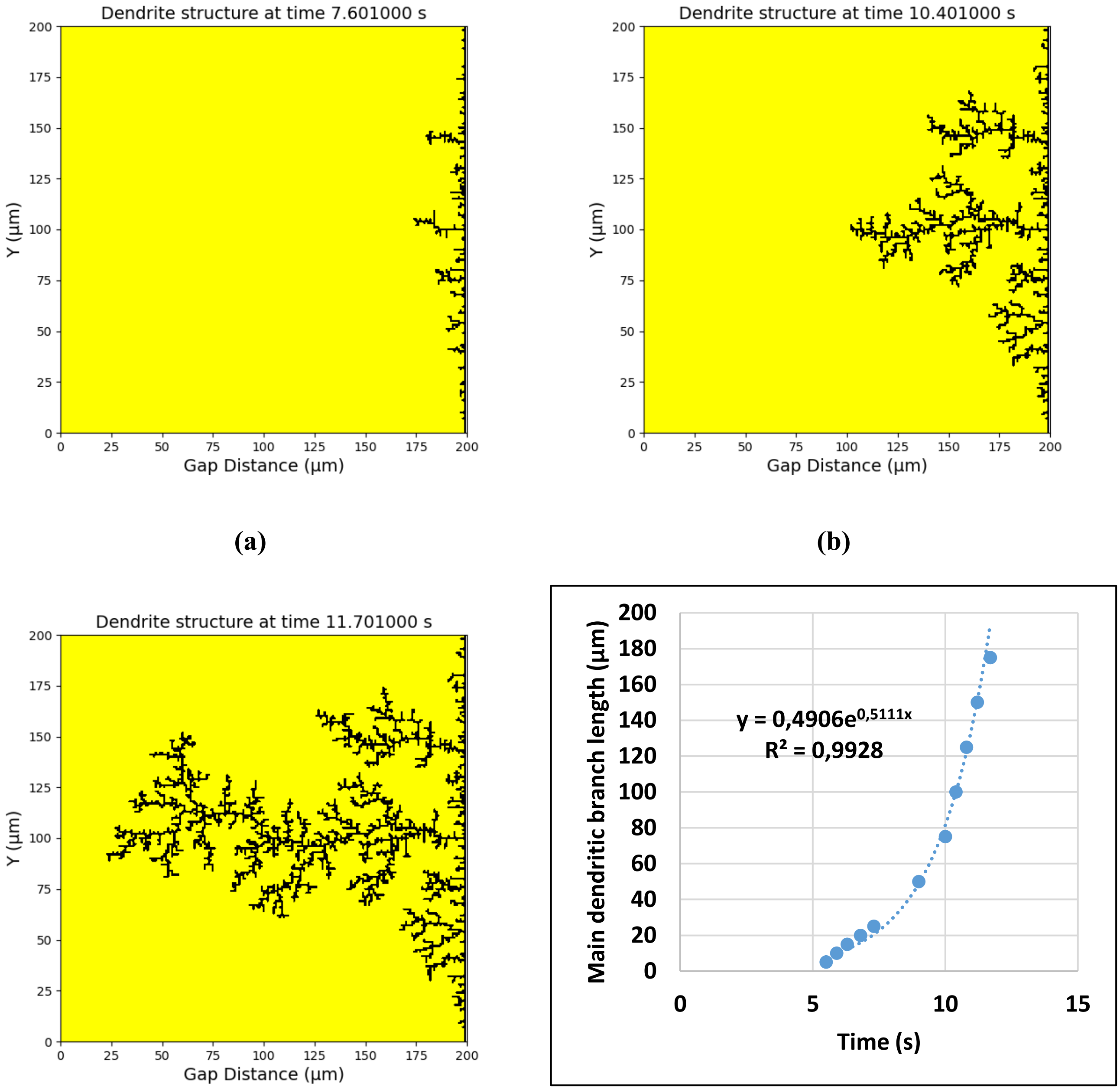

**(a)** **(b)**

**(c)** **(d)**

Fig. 6. Evolution of the main branch length of computed Cu dendrites in the case of N=5, k=1 at: (a) 25 µm, (b) 100 µm, and (c) 175 µm, and (d) Exponential fitting of the main branch length along the gap distance, confirming the exponential growth pattern.

## IV. CONCLUSIONS

The ability of Monte Carlo simulation to model the growth of Cu dendrites during ECM was investigated, focusing on its accuracy in predicting TTF and capturing dendrite morphology as a function of $Cu^{2+}$ ion concentration. The Monte Carlo simulation accounted for two key parameters: the number of dendrite growth attempts per simulation step and the constant for the normalized $Cu^{2+}$ concentration. The lifetime analysis showed that the ECM of Cu is better modeled using a randomized N within a range rather than a fixed deterministic value, confirming the stochastic nature of the ECM process.

The ECM computational model results revealed that the dendrite morphology generally features only one to two dominant dendrites growing within a specific area. This suggests that the primary dendritic branches consume the majority of the surrounding $Cu^{2+}$ ions, regardless of whether the number of dendrite growth attempts is deterministic or random and irrespective of the value of the constant for the normalized $Cu^{2+}$ concentration. Furthermore, the Monte Carlo simulation reveals that as the dendrites approach the anode, they become denser and exhibit a more pronounced fractal-like structure, consistent with experimental observations. Additionally, by fitting the length of the main dendritic branch over time, it is observed that the growth of the computed dendrites follows an exponential pattern. Overall, the proposed model demonstrates strong performance in predicting both TTF and dendrite morphology. However, future work will focus on incorporating experimental deviations to enhance the model's accuracy and reliability.

## ACKNOWLEDGMENT

The research discussed in this paper and carried out at BME has been supported by the National Research, Development and Innovation (NRDI) Office Fund based on the charter of bolster issued by the NRDI Office under the auspices of the Ministry for Innovation and Technology, and by the project FK 138220 and K 145966 of the NRDI Office.

## REFERENCES

[1] X. Zhong, L. Chen, B. Medgyes, Z. Zhang, S. Gao, and L. Jakab, "Electrochemical migration of Sn and Sn solder alloys: A review," *RSC Adv.*, vol. 7, no. 45, pp. 28186–28206, May 2017.

[2] E. L. Lee, Y. S. Goh, A. S. M. A. Haseeb, Y. H. Wong, M. F. MOHD SABRI, and B. Y. Low, "Review—Electrochemical Migration in Electronic Materials: Factors Affecting the Mechanism and Recent Strategies for Inhibition," *J. Electrochem. Soc.*, vol. 170, no. 2, p. 21505, Feb. 2023.

[3] X. Zhong, S. Yu, L. Chen, J. Hu, and Z. Zhang, "Test methods for electrochemical migration: a review," *J. Mater. Sci. Mater. Electron.*, vol. 28, no. 2, pp. 2279–2289, Sep. 2017.

[4] A. Gharaibeh, B. Illes, A. Geczy, and B. Medgyes, "Numerical Models of the Electrochemical Migration: A short review," in *2020 IEEE 26th International Symposium for Design and Technology in Electronic Packaging (SIITME)*, Pitesti, Romania, 2020, pp. 178–183.

[5] X. He, M. H. Azarian, and M. G. Pecht, "Analysis of the kinetics of electrochemical migration on printed circuit boards using Nernst-Planck transport equation," *Electrochim. Acta*, vol. 142, pp. 1–10, Oct. 2014.

[6] B. Illés, B. Medgyes, K. Dušek, D. Bušek, A. Skwarek, and A. Géczy, "Numerical simulation of electrochemical migration of Cu based on the Nernst-Plank equation," *Int. J. Heat Mass Transf.*, vol.

184, p. 122268, Mar. 2022.

[7] H. Ma *et al.*, “Study of electrochemical migration based transport kinetics of metal ions in Sn-9Zn alloy,” *Microelectron. Reliab.*, vol. 83, pp. 198–205, Apr. 2018.

[8] Z. Ható *et al.*, “Electrochemical migration and dendrite growth between two electrodes: Experiments and Brownian dynamics simulations,” *Int. J. Heat Mass Transf.*, vol. 234, p. 126108, Dec. 2024.

[9] C. Cao *et al.*, “A phase-field model of electrochemical migration for silver-based conductive adhesives,” *Electrochim. Acta*, vol. 471, p. 143388, Dec. 2023.

[10] A. Dayoub, A. Gharaibeh, B. Illés, and B. Medgyes, “Insights into copper electrochemical migration through numerical modeling and Monte Carlo simulation,” *Results Eng.*, vol. 25, no. December 2024, p. 103820, Mar. 2025.

[11] B. Medgyes, B. Illés, and G. Harsányi, “Electrochemical migration behaviour of Cu, Sn, Ag and Sn63/Pb37,” *J. Mater. Sci. Mater. Electron.*, vol. 23, no. 2, pp. 551–556, Jun. 2012.

[12] Y. K. Kwok and C. C. K. Wu, “Numerical simulation of electrochemical diffusion-migration model with reaction at electrodes,” *Comput. Methods Appl. Mech. Eng.*, vol. 132, no. 3–4, pp. 305–317, Jun. 1996.

[13] P. Yi, K. Xiao, K. Ding, C. Dong, and X. Li, “Electrochemical migration behavior of copper-clad laminate and electroless nickel/immersion gold printed circuit boards under thin electrolyte layers,” *Materials (Basel).*, vol. 10, no. 2, p. 137, Feb. 2017.

[14] X. Zhong, G. Zhang, Y. Qiu, Z. Chen, and X. Guo, “Electrochemical migration of tin in thin electrolyte layer containing chloride ions,” *Corros. Sci.*, vol. 74, pp. 71–82, Sep. 2013.

[15] J. Diaz and M. J. Grote, “Multi-level explicit local time-stepping methods for second-order wave equations,” *Comput. Methods Appl. Mech. Eng.*, vol. 291, pp. 240–265, Jul. 2015.

[16] F. Jia, M. Chen, Y. Xi, G. Zhang, and C. Yang, “Dynamic characteristics and mechanism of ions migration and dendrites evolution on the printed circuit board surface,” *Exp. Therm. Fluid Sci.*, vol. 163, no. November 2024, p. 111390, Apr. 2025.

[17] A. Gharaibeh, D. Rigler, and B. Medgyes, “Effect of TiO2 Nanoparticles Addition on the Electrochemical Migration of Low-Silver Lead-Free SAC Alloys,” in *2023 46th International Spring Seminar on Electronics Technology (ISSE)*, Timișoara, Romania, 2023, pp. 1–5.

[18] A. Gharaibeh, D. Rigler, and B. Medgyes, “Electrochemical Migration: Evaluating the Effect of Fe2O3 Nanoparticle Incorporation on the Reliability of SAC Alloys,” in *2024 47th International Spring Seminar on Electronics Technology (ISSE)*, Prague, Czech Republic, 2024, pp. 1–6.